Polish Society of Composite Materials
Polskie Towarzystwo Materiałów Kompozytowych

24: 2 (2024) 116-122

COMPOSITES THEORY AND PRACTICE

ISSN (online): 2299-128X

Marek Konieczny

Kielce University of Technology, Faculty of Mechatronics and Mechanical Engineering, Department of Metal Science and Materials Technologies
al. 1000-lecia Państwa Polskiego 7, 25-314 Kielce, Poland
Corresponding author: E-mail: mkon@tu.kielce.pl

Received (Otrzymano) 20.04.2024

PROPERTIES AND STRENGTHENING MECHANISMS OF NICKEL MATRIX COMPOSITES REINFORCED WITH HIGH-SPEED STEEL PARTICLES

https://doi.org/10.62753/ctp.2024.06.2.2

Nickel matrix composites reinforced with T15 high-speed steel (HSS) particles were prepared using powder metallurgy. A systematic investigation was conducted into the effects of the sintering temperature and T15 HSS particle content on the microstructure and properties of the composites. The results indicate that the grain size of the nickel in the composites was effectively refined by the addition of T15 HSS particles in comparison to the pure sintered nickel. It was also observed that the T15 HSS particles, after sintering at all the used temperatures (850, 900 or 950 °C), were diffusion-bonded to the nickel matrix. There were two distinct layers between the reinforced particles and the nickel matrix: the solid solution of elements in nickel and the $FeNi_3$ intermetallic compound, whose thickness slowly grows with the increase in sintering temperature. Also, as the sintering temperature was incremented, the relative density and hardness of the composites gradually rose. When sintered at 950 °C, the Ni+20 wt.%T15 composite achieved a maximum hardness of 135 HB, which was about 52 % higher than that of the pure sintered nickel. The introduction of an increasing amount of T15 HSS particles combined with sintering resulted in a rise in the yield strength of the sintered composites. At all the investigated temperatures, as the T15 HSS particle content was increased, the compressive strength of the composites also gradually grew. Nonetheless, as the sintering temperature was raised from 850 to 950 °C, the compressive strength of the composites initially increased and then decreased. The composite containing 20 wt.%T15 HSS particles sintered at 900 °C achieved the highest compressive strength of 445 MPa, which was about 50 % higher than that of the pure sintered nickel. Additionally, the primary contributions of strengthening mechanisms such as load transfer, grain refinement and thermal expansion mismatch to the mechanical properties of the Ni+T15 HSS composites were analyzed.

Keywords: metal matrix composites, nickel, T15 high-speed steel, mechanical properties, strengthening mechanisms

INTRODUCTION

The demand for composite materials has become a necessity for modern technology, which is why many methods of their production have been developed, for example, by casting or using powder metallurgy [1, 2]. Powder metallurgy (PM) is thought to be the most common production method for metal matrix composites (MMCs) [3]. One of the advantages of PM compared to casting is that it has much better control over the microstructure and distribution of the reinforcement because solid-state diffusion plays a major role in the formation and growth of interparticle bonding [4]. Diffusion itself is dependent on the sintering temperature and time, and has a major effect on the microstructure and mechanical properties. One successful strategy to enhance the mechanical performance of MMCs is second-phase particle strengthening. The particle size and the amount of reinforcement have a pronounced effect on the mechanical properties of composites [5]. The proper addition of reinforcements to metal composites significantly improves their strength, hardness, wear resistance, frictional behavior, creep, and fatigue characteristics, as well as provides an exceptional surface quality in comparison to typical engineering materials [1, 3-7]. Nickel matrix composites (NMCs) are suitable for aerospace and military applications due to their superior mechanical and tribological properties [8]. It is well known that the improvement in the mechanical properties of NMCs mainly depends on the inherent features of the reinforcing phase and its interfacial bonding with the nickel matrix. Although ceramic particles such as carbides [9], borides [10], zirconia [11], and oxides such as Al_2O_3 [12] and ThO_2 [13] are considered to be suitable for the reinforcement phases of nickel matrix composites, as a consequence of their poor wettability and the significant discrepancy in the thermal expansion coefficient between the nickel matrix and ceramic materials, these composite materials lack strength and toughness. It has been also shown [14, 15]

that nickel composites containing transition-metal dichalcogenides (WS_2 and MoS_2) and alkaline halides (CeF_2, BaF_2, and CaF_2) have been extensively used to reduce friction and wear at ambient and high-temperature testing conditions. In order to improve the interfacial bonds and obtain composite materials characterized by high strength and impact strength, a great deal of attention has been paid to metal matrix composites reinforced with metal particles [6, 16]. Nevertheless, there are still few reports on metal particle-reinforced NMCs, and most of them concern the production of nickel matrix composites with soft metals (Au and Ag) used as solid lubricants [10]. The current study uses high-speed steel particles as the reinforcement phase, which have excellent wear resistance, high hardness, and high thermal stability. The main aim is to analyze the effects of the sintering temperature and reinforcement phase content on the microstructure, density, and mechanical properties of the composites. Also, the strengthening mechanisms of the composites were proposed.

EXPERIMENTAL PROCEDURE

In this study, commercially available nickel (99.75 % Ni) and T15 high-speed steel (HSS) powders were used. The chemical composition of T15 HSS powder is shown in Table 1.

TABLE 1. **Chemical composition of T15 HSS powder**

Chemical composition [wt.%]								
C	Si	Mn	Cr	Mo	V	W	Co	Fe
1.5	0.4	0.4	4.5	0.5	5.0	12.5	4.75	rest

Nickel powder with an average particle size of 55 μm was used as the matrix, while T15 HSS powder with particle sizes less than 120 μm was used as the reinforcement. Both the nickel and T15 HSS atomized powder particles had a spherical shape (Fig. 1). The particle size of the nickel powder ranged from 40 to 70 μm and the particle size of the high-speed steel ranged from 50 to 120 μm. Powder mixtures with different amounts of T15 HSS (5, 10, 15, and 20 wt.%) and pure nickel powder were blended in a steel container utilizing a rotary mill with steel balls. The powders were subjected to milling for 1 h using a ball-to-powder ratio (BPR) of 10:1 and 120 rpm as the rotation speed. Cylindrical specimens 20 mm in diameter and 10 mm high made from pure nickel powder and the prepared powder mixtures were subjected to single-track pressing on an Amsler hydraulic press at the compaction pressure of 624 MPa.

The green compacts were sintered at three different temperatures: 850, 900 or 950 °C, in a vacuum furnace for 2 h by applying uniaxial pressure of 5 MPa, and then the furnace was cooled. Specimens intended for microscopic examination were cut transversely using a low-speed diamond saw and then embedded in resin. Next, they were ground with sandpaper with a grit size of up to 1200 and polished with a diamond suspension having a grain size of 1 μm.

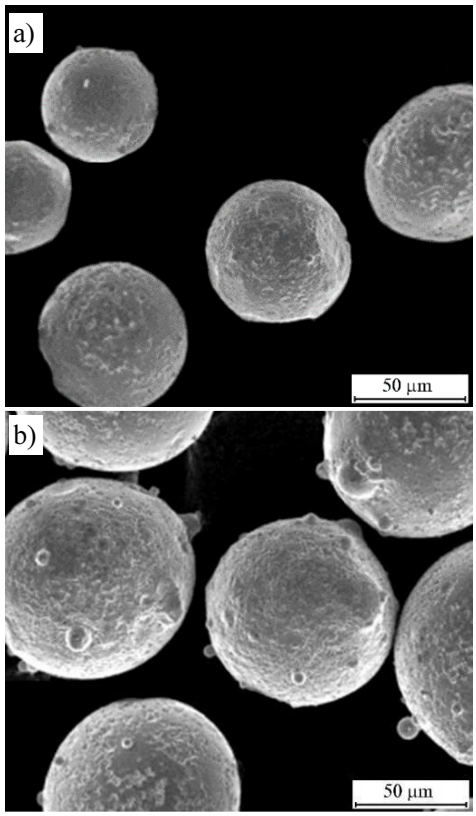

Fig. 1. Scanning electron micrographs of nickel (a) and T15 HSS (b) powders

The microstructure analyses of the prepared metallographic specimens were performed employing a Nikon Eclipse MA200 light microscope (LM) and a JEOL JMS 5400 scanning electron microscope (SEM). Before the samples were examined with the light microscope, they were etched using a solution of 2 mL HNO_3 and 100 mL C_2H_5OH. The grain size of the investigated materials was determined by means of quantitative metallography. The chemical composition of the reaction regions was investigated by energy dispersive X-ray analysis (EDX) utilizing an ISIS 300 (Oxford Instruments). The composition of the phases was determined by comparing the results of the microprobe analysis with the data in the binary phase diagrams [17].

The fabricated materials were subjected to density, hardness, and compression tests. The density of the sintered materials was determined by weighing the specimens in air and water employing WPA120 hydrostatic scales in line with the EN ISO 2738:2001 standard. The hardness of the materials was measured using the Vickers microhardness method (HV0.1) in accordance with the EN ISO 6507-1:2023 standard and the Brinell method with a sintered carbide ball of 5 mm in diameter at a load of 2452 N in accordance with the EN ISO 6506-1:2014 standard. Cubic specimens with a side

length of 10 mm were prepared from the sintered materials and then tested at room temperature under quasi-static compression by means of an Amsler screw machine at the constant crosshead speed of 0.1 mm/min. The reported data for all tests are the average values of three tested specimens.

RESULTS AND DISCUSSION

The introduction of T15 HSS particles into the nickel matrix caused significant changes in the microstructure of the composites. Figure 2 illustrates the metallographic micrographs of the composites containing 5, 10, 15 and 20 wt.% T15 HSS particles sintered at 900 °C.

It can be observed that due to the thorough mixing of the powders before the pressing process, an even distribution of particles in the nickel matrix was achieved. To reveal the microstructure of the T15 HSS particles after sintering, the samples were subjected to an etching process. The annealed high-speed steel microstructure consists of a metal matrix composed of ferrite containing alloying elements and metal carbides. The high-speed steel structure includes M_6C and MC types of carbides [18]. The carbides are visible in the microstructure of the T15 HSS as bright spots on the background of the metal matrix (Fig. 3).

It can also be observed that the T15 HSS particles are diffusion-bonded to the nickel matrix. In order to quantitatively analyze the distribution of each region, point scanning was performed on two different regions of the interface between a T15 HSS particle and the Ni matrix, as shown in Figure 3. There are two clearly visible areas: A and B. The following chemical composition of the region marked A, formed close to the nickel side, was received using SEM and EDX analysis: 97.77 at.% Ni, 1.76 at.% Fe, 0.15 at.% Cr, 0.11 at.% W, 0.08 at.% V, 0.07 at.% Co, and 0.06 at.% of other elements. The results indicate, according to the Fe-Ni diagram [17], the development of a solid solution based on nickel. X-ray microprobe analysis of the region marked B revealed a chemical composition of 76.11 at.% Ni, 22.86 at.% Fe, and 1.03 at.% of other elements, which suggests that an $FeNi_3$ intermetallic compound was formed. It was discovered that the contents of elements Ni, Fe, W, Cr and V vary greatly in different regions, which means that there is mutual diffusion between the Ni matrix and T15 HSS particles.

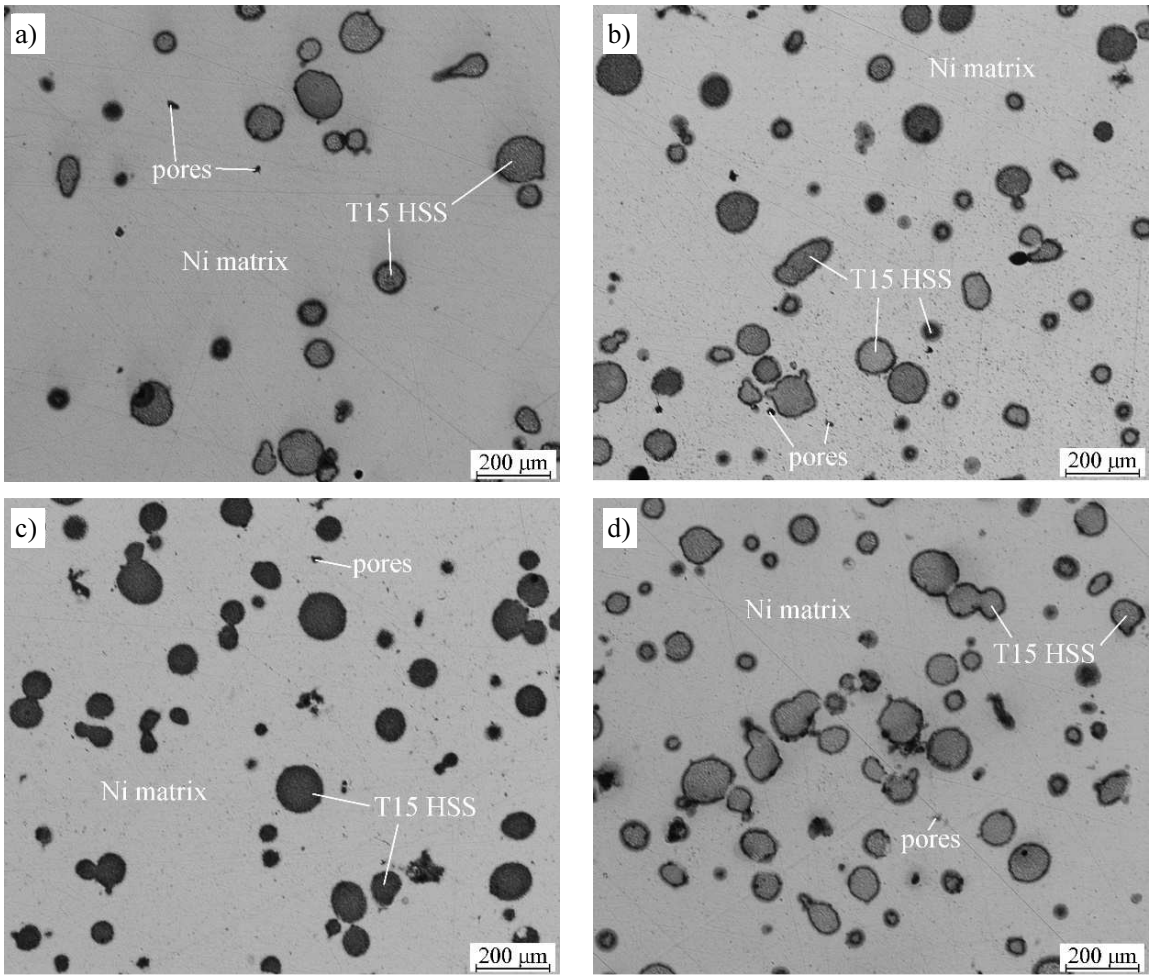

Fig. 2. LM micrographs of composites containing 5 (a), 10 (b), 15 (c) and 20 wt.% T15 HSS particles (d) sintered at 900 °C

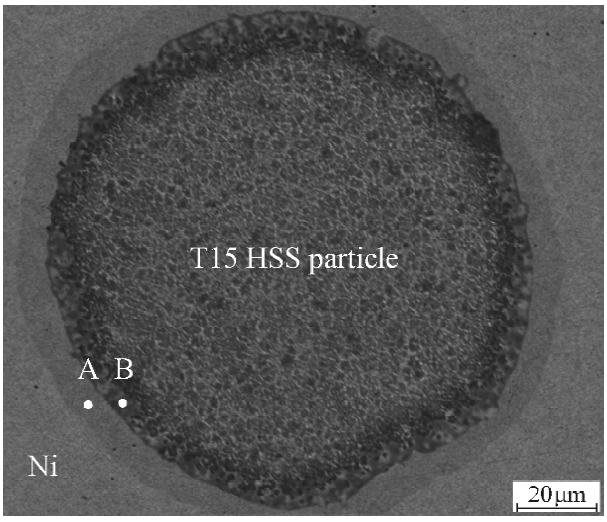

Fig. 3. SEM micrograph of T15 HSS particle-Ni matrix region of composite sintered at 950 °C

The thickness of the diffusion-bonded zone depended on the sintering temperature. It was approximately 12 μm when sintered at the temperature of 850 °C, 16 μm at 900 °C, and 18 μm at 950 °C. Furthermore, as the sintering temperature was increased, the number of pores gradually decreased, and the relative density of the sintered nickel as well as of all the investigated composites grew (Table 2).

TABLE 2. **Density of sintered nickel and composites**

Material	Sintering temperature [°C]	Measured density [g/cm^3]	Relative density [%]
Ni	850	8.411±0.03	94.51
Ni+5%T15	850	8.338±0.04	94.11
Ni+10%T15	850	8.302±0.05	94.02
Ni+15%T15	850	8.250±0.04	93.86
Ni+20%T15	850	8.176±0.07	93.55
Ni	900	8.518±0.04	95.71
Ni+5%T15	900	8.424±0.06	95.08
Ni+10%T15	900	8.381±0.03	94.92
Ni+15%T15	900	8.284±0.05	94.25
Ni+20%T15	900	8.222±0.02	94.08
Ni	950	8.655±0.04	97.25
Ni+5%T15	950	8.574±0.05	96.78
Ni+10%T15	950	8.490±0.07	96.15
Ni+15%T15	950	8.427±0.03	95.88
Ni+20%T15	950	8.326±0.04	95.27

The examinations also showed that the introduction of the T15 HSS particles (theoretical density 8.19 g/cm^3) into the nickel matrix (theoretical density 8.9 g/cm^3) resulted in an obvious decline in the density of the composites. The theoretical densities of the composites containing 5, 10, 15, and 20 wt.% T15 HSS particles are 8.86, 8.83, 8.78, and 8.74 g/cm^3, respectively. Most of the visible pores in the microstructures (Fig. 2) were distributed at the interfaces between the nickel matrix and the reinforced particles. The average grain size of the nickel matrix in the composites sintered at 850, 900 and 950 °C was 1.85±0.11, 2.27±0.16 and 2.69 ±0.21 μm, respectively. Similar measurements performed for pure nickel sintered at 850, 900 and 950 °C showed that the average grain size was 2.55±0.17, 3.87±0.13 and 4.37±0.19 μm, respectively. It is obvious that as the sintering temperature was raised, the grain size gradually increased, but in the composites, the T15 HSS particles effectively prevented grain growth by pinning the grain boundary, leading to a smaller nickel grain structure. This phenomenon is also connected to the particle content in the composites. It was noticed that the higher the content of particles, the smaller the average grain size of the nickel matrix. This is because a smaller nickel grain structure is in the vicinity of the T15 HSS particles and a relatively larger grain size in the areas further away from the reinforcing particles.

The Vickers indentation test was carried out on various sections of the composite to analyze the change in microhardness from the Ni matrix to the T15 HSS particles (Fig. 4)

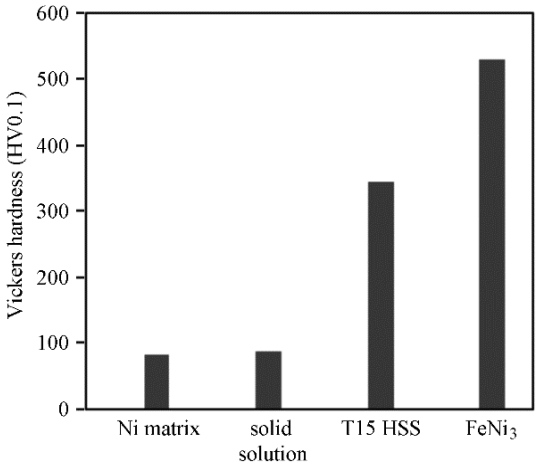

Fig. 4. Microhardness of various regions of Ni-T15 HSS composite

The microhardness of the T15 HSS particles (345±15 HV0.1) and $FeNi_3$ intermetallic phase (530 ±20 HV0.1) is about 4.2 and 6.5 times higher than that of the pure nickel and solid solution based on nickel, respectively. Table 3 displays the Brinell hardness of the pure nickel and the composites sintered at various temperatures.

When the sintering temperature of the pure nickel was increased from 850 to 900 °C, a denser material was obtained and the Brinell hardness increased. Nonetheless, when the sintering temperature was raised from 900 to 950 °C, the grain size of the pure nickel grew rapidly, and therefore the Brinell hardness started to dwindle.

TABLE 3. **Brinell hardness and compressive strength of sintered Ni and composites**

Material	Sintering temperature [°C]	Brinell hardness [HBW]	Compressive strength [MPa]
Ni	850	82±1.5	285±5
Ni+5%T15	850	88±1.6	328±6
Ni+10%T15	850	94±1.4	351±4
Ni+15%T15	850	102±1.3	390±7
Ni+20%T15	850	115±1.5	417±3
Ni	900	84±1.2	298±4
Ni+5%T15	900	93±1.3	342±5
Ni+10%T15	900	101±1.6	368±2
Ni+15%T15	900	116±1.8	402±5
Ni+20%T15	900	128±1.4	445±8
Ni	950	83±1.7	292±4
Ni+5%T15	950	96±1.6	336±1
Ni+10%T15	950	108±1.2	359±6
Ni+15%T15	950	121±1.7	394±7
Ni+20%T15	950	135±1.0	425±3

The hardness of the composites rose constantly with increasing sintering temperatures. It was also found that the hardness grew with the addition of more reinforcement. This is resulted in the higher hardness values of the T15 HSS and $FeNi_3$ as compared to the nickel matrix. This higher hardness is also attributed to the decrease in the interparticle distance with the increment in the amount of reinforcement, as represented by Equation (1)

$$d_i = r_p \left[\left(\frac{\pi}{6V_f} \right)^{\frac{1}{3}} - 1 \right] \tag{1}$$

where d_i, r_p, and V_f are the inter-particle distance, radius of the particle, and volume fraction of reinforcement, respectively [19]. The reasons for the improvement in the Brinell hardness of the composites are as follows: (a) the density of the composites grew as a result of the higher sintering temperatures; (b) the T15 HSS particles with high hardness were dispersed in the nickel matrix; (c) the addition of the T15 HSS particles led to grain refinement; and (d) a hard secondary phase ($FeNi_3$) was observed in the microstructure. For example, at the same sintering temperature (950 °C), the hardness of the Ni+20%T15 composite is about 52 % higher than that of the pure sintered nickel. Figure 5 presents the exemplary room-temperature compressive stress-strain curves for the composites sintered at 900 °C.

The introduction of an increasing amount of T15 HSS particles combined with sintering resulted in a rise in the yield strength of the sintered composites. Under compressive loading, according to Kim et al. [20], the reinforcement particles move in the loading direction to become closer to each other, and deformation takes place mainly in the matrix. Therefore, the plastic deformability of the sintered composites decreased with the increment in the amount of reinforced particles. Table 3 displays the compressive strength of the pure nickel and the Ni+T15 HSS composites sintered at various temperatures. At all the investigated temperatures, as the T15 HSS particle content was increased, the compressive strength of the composites also gradually grew. However, as the sintering temperature was increased, the compressive strength of the composites initially rose and then dropped. When the sintering temperature was incremented from 850 to 900 °C, a denser material was obtained, and the compressive strength grew. Nevertheless, when the sintering temperature was raised from 900 to 950 °C, the grain size of the nickel matrix increased, and therefore the compressive strength of the composites started to fall. The composite containing 20 wt.%T15 HSS particles sintered at 900 °C achieved the highest compressive strength of 445 MPa, which was about 50 % higher than that of the pure sintered nickel.

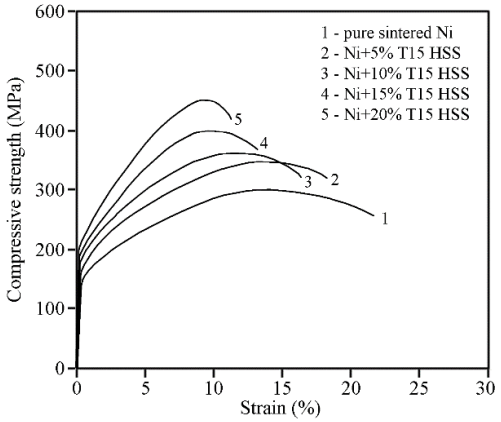

Fig. 5. Compressive stress-strain curves for Ni+T15 HSS composites sintered at 900°C

The second-phase particles can strengthen the composites mainly by means of the following mechanisms: Orowan strengthening (when the reinforcing particles are smaller than 1 μm and closely spaced, hence in this case the contribution of Orowan strengthening to the composite can be ignored), load transfer strengthening, grain refinement strengthening and coefficient of thermal expansion (CTE) mismatch strengthening [21]. Load transfer strengthening refers to the transfer of load from the softer nickel matrix to the harder T15 HSS reinforcing particle during the loading process. The contribution of load transfer strengthening to the strength of the composites can be estimated by the following formula:

$$\Delta\sigma_{Load} = 0.5 f_{T15} \sigma_m \tag{2}$$

where σ_m is the yield strength of the nickel matrix and f_{T15} is the volume fraction of the T15 HSS particles. The volume fraction of the T15 HSS particles can be calculated from the mass fraction using the formula:

$$f_{T15} = \frac{\frac{wt.\%\,T15}{\rho_{T15}}}{\frac{wt.\%T15}{\rho_{T15}} + \frac{wt.\%Ni}{\rho_{Ni}}} \quad (3)$$

The contribution of grain refinement to strength can be calculated using the Hall-Petch equation:

$$\Delta\sigma_{H-P} = k_{Ni}\left(d_c^{-0.5} - d_{Ni}^{-0.5}\right) \quad (4)$$

where k_{Ni} is the Hall-Petch constant (for Ni, k_{Ni} = = 0.158 MPa·m$^{1/2}$), d_c and d_{Ni} are the average grain sizes of the Ni+T15 HSS composites and pure nickel. The volumetric strain between the reinforcing particles, the hard secondary phase ($FeNi_3$) around the particles, and the nickel matrix during sample cooling is caused by a mismatch in CTE, which improves the yield strength by producing dislocations surrounding the reinforced particles. There is a noticeable CTE mismatch between the T15 HSS particles, the $FeNi_3$ intermetallic compound, and the nickel matrix. The CTE of T15 HSS is $9.9 \cdot 10^{-6}$ K^{-1}, the CTE of $FeNi_3$ is $18 \cdot 10^{-6}$ K^{-1}, and the CTE of nickel is $12.7 \cdot 10^{-6}$ K^{-1} [22]. The thermal mismatch contribution can be estimated using the following formula:

$$\Delta\sigma_{CTE} = 1.25Gb\sqrt{\frac{12f_{T15}\Delta T\Delta CTE}{bd}} \quad (5)$$

where G is the shear modulus of Ni (76 GPa), b is the Burger's vector of Ni (0.2492 nm) [23], f_{T15} is the volume fraction of T15 HSS, ΔT is the difference between the sintering temperature and room temperature, ΔCTE is the CTE mismatch between the $FeNi_3$ layer around the T15 HSS particles and nickel, and d is the average particle size of the T15 HSS particles. The superposition relationship is mainly applied to the research of metal matrix composites reinforced with micron-sized particles [21]. The theoretical yield strength of the Ni+T15 HSS composites can be estimated as follows:

$$\sigma_{th} = \sigma_m + \Delta\sigma_{H-P} + \sqrt{\Delta\sigma_{Load}^2 + \Delta\sigma_{CTE}^2} \quad (6)$$

where σ_m is the yield strength of the nickel matrix (142 MPa), while $\Delta\sigma_{H\text{-}P}$, $\Delta\sigma_{Load}$, and $\Delta\sigma_{CTE}$ denote the strength contributions from the grain refinement, load transfer and thermal mismatch. The predicted theoretical values of most of the specimens coincided well with the experimental values.

CONCLUSIONS

In this paper, Ni+T15 HSS composites were prepared using powder metallurgy techniques. The study investigated the effects of the sintering temperature and particle content on the microstructure, density, and mechanical properties of the composites. The main conclusions are as follows:

1. The addition of T15 HSS particles effectively inhibits the growth of the nickel grains, and the grain size is proportional to the sintering temperature.
2. The T15 HSS particles, after sintering at all the investigated temperatures, are diffusion-bonded to the nickel matrix. There are two distinct layers between the reinforcing particles and the nickel matrix: the solid solution in nickel and the $FeNi_3$ intermetallic compound.
3. The hardness and density of the Ni+T15 HSS composites grow with increasing temperature. The highest hardness of 135 HB was achieved by the Ni+20 wt.%T15 HSS composite after sintering at 950 °C, which is about 52 % higher than that of the pure sintered nickel.
4. The introduction of increasing amounts of T15 HSS particles combined with sintering results in a rise in the yield strength of the composites. As the sintering temperature is increased from 850 to 950 °C, the compressive strength of the composites initially grows and then drops. The composite containing 20 wt.%T15 HSS particles sintered at 900 °C achieved the highest compressive strength of 445 MPa, which is about 50 % higher than that of the pure sintered nickel.
5. Grain refinement, thermal expansion coefficient mismatch, and load transfer strengthening are the main strengthening mechanisms for the Ni+T15 HSS composites.

REFERENCES

[1] Sharma D., Mahant D., Upadhyay G., Manufacturing of metal matrix composites: A state of review, Materials Today: Proceedings 2020, 26, 506-519, DOI: 10.1016/j.matpr.2019.12.128.

[2] Sankhla A., Patel K., Metal matrix composites fabricated by stir casting process – A review, Advances in Materials and Processing Technologies 2022, 8, 1270-1291, DOI: 10.1080/2374068X.2020.1855404.

[3] Qu X., Zhang L., Wu M., Ren S., Review of metal matrix composites with high thermal conductivity for thermal management applications, Progress in Natural Science: Materials International 2011, 21, 189-197, DOI: 10.1016/S1002-0071(12)60029-X.

[4] Srivastava A., Dixit A., Tiwari S., A review on the intensification of metal matrix composites and its nonconventional machining, Science and Engineering of Composite Materials 2018, 25, 213-228, DOI: 10.1515/secm-2015-0287.

[5] Konieczny M., The effect of sintering temperature, sintering time and reinforcement particle size on properties of Al-Al_2O_3 composites, Composites Theory and Practice 2012, 12, 39-43.

[6] Kargul M., Konieczny M., Copper matrix composites reinforced with steel particles, AIMS Materials Science 2021, 8, 321-342, DOI: 10.3934/matersci.2021021.

[7] Szewczyk-Nykiel A., Microstructure and properties of sintered metal matrix composites reinforced with SiC particles, Technical Transactions 2017, 6, 179-190, DOI: 10.4467/2353737XCT.17.098.6574.

[8] Kumar B., Ananthaprasad G., Krishna K., A review on mechanical and tribological behaviors of nickel matrix composites, Indian Journal of Science and Technology 2016, 9, 1-7, DOI: 10.17485/ijst/2016/v9i2/82868.

[9] Leech P., Li X., Alam N., Comparison of abrasive wear of a complex high alloy hard facing deposit and WC-Ni based metal matrix composite, Wear 2012, 294-295, 380-386, DOI: 10.1016/j.wear.2012.07.015.

[10] Tyagi R., Xiong D., Li J., Dai J., Elevated temperature tribological behavior of Ni based composites containing nano-silver and hBN, Wear 2010, 269, 884-890, DOI: 10.1016/j.wear.2010.08.022.

[11] El-Wazery M., El-Desouk A., Hamed O., Fathy A., Mansour N., Electrical and mechanical performance of zirconia-nickel functionally graded materials, International Journal of Engineering Transactions A: Basics 2013, 26, 375-382, DOI: 10.5829/idosi.ije.2013.26.04a.06.

[12] Karayannis V., Moutsatsou A., Synthesis and characterization of nickel-alumina composites from recycled nickel powder, Advances in Materials Science and Engineering 2012, 395612, DOI: 10.1155/2012/395612.

[13] Yamada T., Nickel-base composite materials and their bonding, Welding International 1990, 4, 593-599.

[14] Li F., Cheng J., Zhu S., Hao J., Yang J., Liu W., Microstructure and mechanical properties of Ni-based high-temperature solid-lubricating composites, Materials Science and Engineering A 2017, 682, 475-481, DOI: 10.1016/j.msea.2016.11.069.

[15] Tabrez S., Gaur K., Kumar V., Jha P., Nautiyal H., Salam A., Singh S., Nickel metal matrix composites reinforced with solid lubricants: A comprehensive review, Materials Today: Proceedings 2023, in press, DOI: 10.1016/j.matpr.2023.07.081.

[16] Xue M., Tribological behaviour of Ni-Cr based composite at high temperature, Transaction of Non Ferrous Metals Society of China 2007, 17, 570-574.

[17] Predel B., Phase Equilibria, Crystallographic and Thermodynamic Data of Binary Alloys, Springer, Berlin 1994, DOI: 10.1007/b47753.

[18] Serna M., Jesus E., Galego E., Martinez L., An overview of the microstructure present in high speed steel carbides crystallography, Materials Science Forum 2006, 530, 48-52, DOI: 10.4028/www.scientific.net/MSF.530-531.48.

[19] Vani V., Chak S., The effect of process parameters in aluminum metal matrix composites with powder metallurgy, Manufacturing Review 2018, 5, 7-20, DOI: 10.1051/mfreview/2018001.

[20] Kim H., Hong S., Kim S., On the rule of mixtures for predicting the mechanical properties of composites with homogenously distributed soft and hard particles, Journal of Materials Processing Technology 2001, 112, 109-113, DOI: 10.1016/S0924-0136(01)00565-9.

[21] Cai C., He S., Li L., Teng Q., Song B., Yan C., Wei Q., Shi Y., In-situ TiB/Ti-6Al-4V composites with a tailored architecture produced by hot isostatic pressing: Microstructure evolution, enhanced tensile properties and strengthening mechanisms, Composites Part B: Engineering 2019, 164, 546-558, DOI: 10.1016/j.compositesb.2019.01.080.

[22] Pandya N., Mevada A., Gajjar P., Lattice dynamical and thermodynamic properties of $FeNi_3$, FeNi and Fe_3Ni invar materials, Computational Materials Science 2016, 123, 287--295, DOI: 10.1016/j.commatsci.2016.07.001.

[23] Csiszár G., Pantleon K., Alimadadi H., Ribárik G., Ungár T., Dislocation density and Burgers vector population in fiber-textured Ni thin films determined by high-resolution X-ray line profile analysis, Journal of Applied Crystallography 2012, 45, 61-70, DOI: 10.1107/S0021889811053234.

